



HAL
open science

Plasmonic properties of implanted Ag nanoparticles in SiO₂ thin layer by spectroscopic ellipsometry

Yann Battie, Aotmane En Naciri, Nouari Chaoui, Yann Le Gall, Dominique Muller, Marzia Carrada, Daniel Mathiot

► **To cite this version:**

Yann Battie, Aotmane En Naciri, Nouari Chaoui, Yann Le Gall, Dominique Muller, et al.. Plasmonic properties of implanted Ag nanoparticles in SiO₂ thin layer by spectroscopic ellipsometry. *Journal of Applied Physics*, 2017, 122 (8), pp.085308. 10.1063/1.4989793 . hal-01755345

HAL Id: hal-01755345

<https://hal.science/hal-01755345v1>

Submitted on 5 Apr 2018

HAL is a multi-disciplinary open access archive for the deposit and dissemination of scientific research documents, whether they are published or not. The documents may come from teaching and research institutions in France or abroad, or from public or private research centers.

L'archive ouverte pluridisciplinaire **HAL**, est destinée au dépôt et à la diffusion de documents scientifiques de niveau recherche, publiés ou non, émanant des établissements d'enseignement et de recherche français ou étrangers, des laboratoires publics ou privés.

Plasmonic properties of implanted Ag nanoparticles in SiO₂ thin layer by spectroscopic ellipsometry

Yann Battie, Aotmane En Naciri, Nouari Chaoui, Yann Le Gall, Dominique Muller, Marzia Carrada, and Daniel Mathiot

Citation: *Journal of Applied Physics* **122**, 085308 (2017); doi: 10.1063/1.4989793

View online: <https://doi.org/10.1063/1.4989793>

View Table of Contents: <http://aip.scitation.org/toc/jap/122/8>

Published by the [American Institute of Physics](#)

Articles you may be interested in

[Antiferromagnetic anisotropy determination by spin Hall magnetoresistance](#)

Journal of Applied Physics **122**, 083907 (2017); 10.1063/1.4986372

[Enhanced room temperature ferromagnetism in Ni doped SnO₂ nanoparticles: A comprehensive study](#)

Journal of Applied Physics **122**, 083906 (2017); 10.1063/1.4999830

[Photo-assisted Kelvin probe force microscopy investigation of three dimensional GaN structures with various crystal facets, doping types, and wavelengths of illumination](#)

Journal of Applied Physics **122**, 085307 (2017); 10.1063/1.5000137

[Operator-sum models of quantum decoherence in molecular quantum-dot cellular automata](#)

Journal of Applied Physics **122**, 084304 (2017); 10.1063/1.4993450

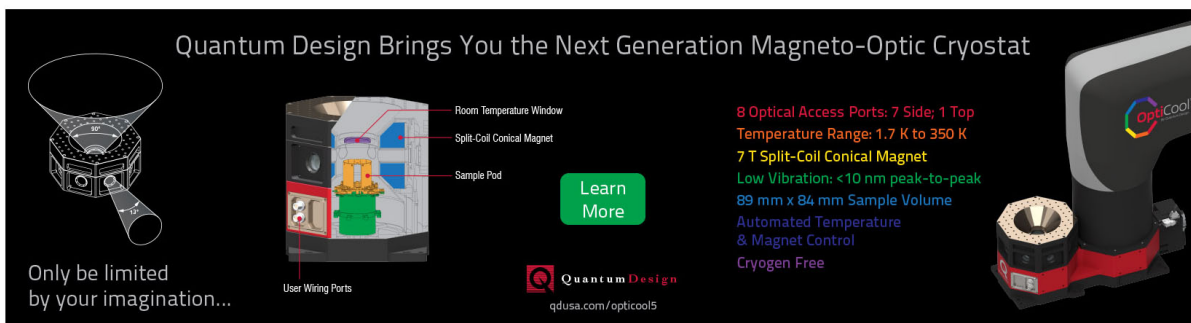
[Formation of nitrogen oxides from atmospheric electrodeless microwave plasmas in nitrogen–oxygen mixtures](#)

Journal of Applied Physics **122**, 083303 (2017); 10.1063/1.4996790

[Effects of ultrathin coating on the tensile behavior of nanoporous gold](#)

Journal of Applied Physics **122**, 084305 (2017); 10.1063/1.5000368

Quantum Design Brings You the Next Generation Magneto-Optic Cryostat



The advertisement features a central cutaway diagram of the cryostat with labels: Room Temperature Window, Split-Coil Conical Magnet, Sample Pod, and User Wiring Ports. To the left is a 3D perspective view of the device. To the right is a photograph of the physical cryostat with the 'OptiCool' logo. A 'Learn More' button is positioned in the center.

Only be limited by your imagination...

Learn More

Quantum Design
qdusa.com/opticool5

8 Optical Access Ports: 7 Side; 1 Top
Temperature Range: 1.7 K to 350 K
7 T Split-Coil Conical Magnet
Low Vibration: <10 nm peak-to-peak
89 mm x 84 mm Sample Volume
Automated Temperature & Magnet Control
Cryogen Free

Plasmonic properties of implanted Ag nanoparticles in SiO₂ thin layer by spectroscopic ellipsometry

Yann Battie,¹ Aotmane En Naciri,^{1,a)} Nouari Chaoui,¹ Yann Le Gall,² Dominique Muller,² Marzia Carrada,³ and Daniel Mathiot²

¹LCP-A2MC, Institut Jean Barriol, Université de Lorraine, 1, Bd Arago, 57070 Metz, France

²ICube, Université de Strasbourg-CNRS, 23 rue du Loess BP20, 67037 Strasbourg Cedex 2, France

³CEMES-CNRS, nMat Group, 29 rue J. Marvig, 31055 Toulouse, France

(Received 12 June 2017; accepted 13 August 2017; published online 28 August 2017)

We report an uncommon study of the insertion of distributions of both volume fraction and depolarization factors in the modeling of the plasmonic properties of implanted Ag nanoparticles (Ag-NPs) in a SiO₂ layer when using spectroscopic ellipsometry (SE) characterization. The Ag-NPs were embedded in the SiO₂ matrix by Ag⁺ ion implantation at various doses of 0.5×10^{16} , 1×10^{16} , 2×10^{16} , and 5×10^{16} ions cm⁻². The formation of the Ag-NPs in a host matrix of SiO₂ was controlled by transmission electron microscopy (TEM). The Ag-NPs are self-organized in the layer, and their mean radius ranges between 2 and 20 nm. The optical properties of layers were extracted by modeling the SE parameters by taking into account the depth profile concentration of Ag-NPs. The mixture of SiO₂ and Ag-NP inclusions was modeled as an effective medium according to the shape distributed effective medium theory (SDEMT). In addition to the optical responses, it is shown that this model enables the explanation of the impact of NP shape distribution on the plasmon band and provides precious information about the NP shape characteristics. A good agreement was obtained between ellipsometry and TEM results. The distribution of the volume fraction in the film was found to lead to a gradient of effective dielectric function which was determined by the SDEMT model. The effective dielectric function reveals distinct Ag plasmon resonance varying as the Ag⁺ ions dose is varied. The real part of the dielectric function shows a significant variation around the plasmon resonance in accordance with the Kramers-Kronig equations. All determined optical parameters by SDEMT are provided and discussed. We highlight that SE combined with SDEMT calculations can be considered as a reliable tool for the determination of the NP shape and volume fraction distributions without the need of TEM. *Published by AIP Publishing.*

[<http://dx.doi.org/10.1063/1.4989793>]

I. INTRODUCTION

One of the most fascinating varieties of nanomaterials is composite layer containing metallic nanoparticles (NPs) which now are considered as a fundamental for designing new applications in photonics, optoelectronics, and nonlinear optics.^{1,2}

Several chemical and physical methods are currently used for the fabrication of such composite layers, see, for example, Ref. 3. Standing apart from the rest, the ion implantation technique enables us to introduce high concentrations as well as different metals into the near surface regions of the dielectric layers.⁴⁻⁶ The formation of NPs by the ion implantation technique in the layer depends on its own properties, as well as on the ion implantation parameters (ion dose and energy, target and annealing temperature, etc.).⁷ Generally, the depth distribution of implanted ions and their penetration in the layer-target are studied by various physical profiling techniques like Rutherford Backscattering Spectroscopy (RBS) or Secondary Ion Mass Spectroscopy (SIMS) and by computer simulation such as SRIM.⁸ However, these methods are not able to provide other relevant information, which

could be helpful to optimize the optical properties of the material.

In this paper, we show that spectroscopic ellipsometry (SE) is a valuable tool to determine both the optical properties of the composite layer and the depth distribution of nanoparticles formed by implantation. Since the knowledge of the effective dielectric function of nano-composite film is a crucial issue to design optical devices, this work is devoted to a detailed study of the optical properties of Ag nanoparticles (Ag-NPs) embedded in a SiO₂ matrix by spectroscopic ellipsometry. The mixture of Ag-NP inclusions and silica was modeled as an effective medium according to the shape distributed effective medium theory (SDEMT) introduced to describe the optical properties of spheroids distributed in shape.⁹⁻¹¹ We show in this study that the SDEMT model, based on a mean field and quasistatic approach, enables the explanation of the strong correlation between the shape distribution and the plasmon band. Previously, SDEMT was successfully used to study the extinction spectra of metallic colloidal solutions⁹⁻¹¹ and to determine the morphology of gold NPs in a photoresist film.¹² Here, the SDEMT is used to analyze the ellipsometric parameters with the additional difficulty of the consideration of the depth profile concentration of Ag-NPs in the SiO₂ layer. The distribution of the volume

^{a)}Author to whom correspondence should be addressed: aotmane.en-naciri@univ-lorraine.fr

fraction in the film was found to lead to a gradient of the effective dielectric function of the nano-composite layer which is discussed in detail throughout this report. Finally, the main purpose of this article is to show that SE combined with SDEMT calculations can be considered as a reliable tool for the determination of the NP shape and to probe the variations of the NP concentration in the film depth without the need of transmission electron microscopy (TEM).

II. EXPERIMENTAL

A. Sample details

First of all, Si substrates were oxidized in dry O₂ to form a 250 nm thick SiO₂ layer, as checked by ellipsometry. These wafers were then implanted with Ag⁺ ions at 180 keV, at various doses of 0.5×10^{16} , 1×10^{16} , 2×10^{16} , and 5×10^{16} cm⁻². In order to minimize self-heating during the implantation, the wafers were mounted on a sample holder cooled down by flowing of cold water. These wafers were then cut into individual samples of about 1.5×1.5 cm⁻². Some samples were then annealed for 30 minutes at various temperatures between 300 and 500 °C. The names used for the different samples, as a function of their detailed preparation parameters (Ag⁺ dose and annealing temperature), are indicated in Table I. The names of the samples are given as Dx-T, where x denotes the ion dose ($\times 10^{16}$ cm⁻²) and T denotes the annealing temperature.

As expected by SRIM simulations and confirmed by our RBS measurement (not shown here), the implantation conditions lead to Ag profiles entirely confined inside the oxide layer, up to a depth of about 170 nm, with a maximum concentration of 3 to 10% depending on the implanted dose.

The effective formation of the Ag-NPs was checked by transmission electron microscopy (TEM). Typical examples are given in Fig. 1 for the two highest doses as a function of the post-anneal treatment. The first interesting point to note (Fig. 1) is that the Ag-NPs are formed during the ion implantation step, without any subsequent annealing. It is also found that the effect of annealing temperature is significantly smaller than that of the implanted dose. Of course, as expected, their size is strongly dependent on the Ag implantation dose, lower doses leading to smaller sizes.

Figure 1 also evidences that the oxide thickness of the implanted samples (270 nm) is significantly higher than the starting one (250 nm). This simply means that the swelling of the SiO₂ layer induced by implantation and the Ag-NPs growth over-compensates the thinning due to the sputtering linked to the high dose Ag implantation.

Since the main purpose of this work is not to investigate in detail the mechanism of the Ag-NP formation, we will not comment later on the exact origin of the Ag-NP distribution in the samples. We just want to summarize the main results, relevant for the detailed analysis of the SE results performed below: Our experimental process leads to well defined spherical NPs exhibiting a volume fraction distribution within the layer, with a maximum concentration at a depth of around 75 nm from the surface. The NPs are more or less self-organized within the layer, and their mean radius ranges between 2 and 20 nm. We note that the spatial self-organization of NPs could occur during the relaxation by nucleation and Ostwald ripening.^{13–15}

B. Ellipsometry measurements and modeling details

1. Ellipsometry

Ellipsometry measures the changes in the polarization state between incident and reflected light on the samples. The measured values are the ψ and Δ ellipsometric angles. They are related to the ratio of the Fresnel amplitude reflection coefficients of the sample, r_p and r_s , respectively, for p-polarized (parallel to the plane of incidence) and s-polarized light (perpendicular to the plane of incidence) by¹⁶

$$r_p/r_s = \tan(\psi) e^{i\Delta}. \quad (1)$$

The spectroscopic measurements are performed in air at room temperature using a photoelastic modulator ellipsometer (UVISEL). This ellipsometer measures the I_c and I_s parameters related to the ellipsometric angles by

$$I_c = \sin(2\psi) \cos(\Delta) \quad \text{and} \quad I_s = \sin(2\psi) \sin(\Delta). \quad (2)$$

Variable angle SE measurements on the Ag-implanted SiO₂ films are performed in air at room temperature at angles of incidence of 50°, 60°, and 70° in the 1.5–4.5 eV energy range. The measured ellipsometric parameters of all samples are reported in Fig. 2 for the I_c parameter and in Fig. 3 for the I_s parameter. The observed oscillations in these figures are the result of the interference phenomena related to the multi-reflection in the silica layer. The same I_c and I_s behaviors are obtained for the samples obtained from the same dose, irrespective of their subsequent annealing, confirming that, as already mentioned above, the effect of annealing on the size distribution of the Ag-NPs is insignificant.

In order to be more quantitative and to extract the optical responses of the embedded Ag-NPs in the silica layer, a

TABLE I. Characteristics and names of different samples used in the study.

Sample name	D5-RT	D5-300	D5-400	D5-500
Dose (ions cm ⁻²);T(°C)	5×10^{16} ;23	5×10^{16} ;300	5×10^{16} ;400	5×10^{16} ;500
Sample name	D2-RT	D2-300	D2-400	D2-500
Dose (ions cm ⁻²);T(°C)	2×10^{16} ;23	2×10^{16} ;300	2×10^{16} ;400	2×10^{16} ;500
Sample name	D1-RT	D1-300	D1-400	D1-500
Dose (ions cm ⁻²);T(°C)	1×10^{16} ;23	1×10^{16} ;300	1×10^{16} ;400	1×10^{16} ;500
Sample name	D0.5-RT	D0.5-300	D0.5-400	D0.5-500
Dose (ions cm ⁻²);T(°C)	5×10^{15} ;23	5×10^{15} ;300	5×10^{15} ;400	5×10^{15} ;500

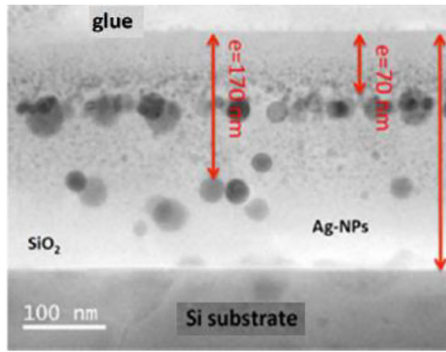
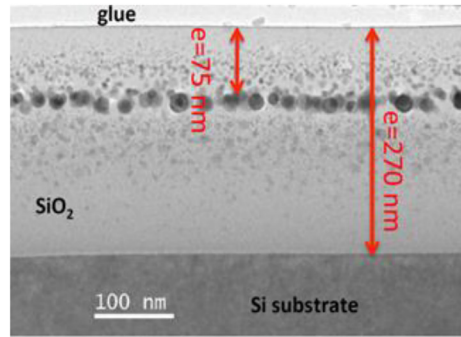
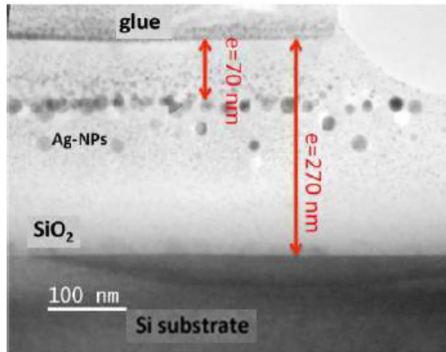
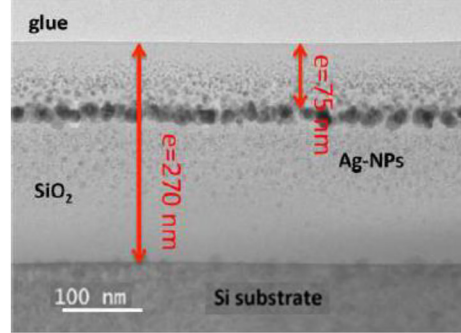
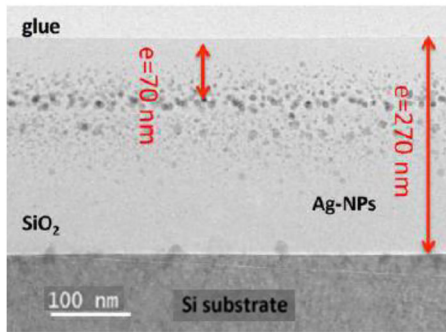
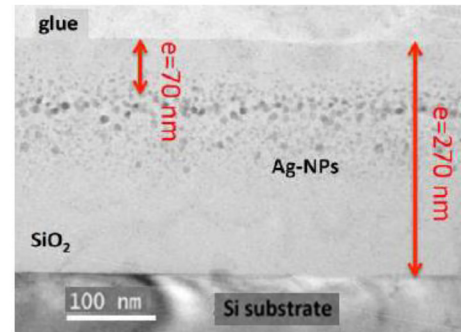
(a) D5-RT ($5 \times 10^{16} \text{ cm}^{-2}$, 23°C)(b) D5-300 ($5 \times 10^{16} \text{ cm}^{-2}$, 300°C)(c) D5-400 ($5 \times 10^{16} \text{ cm}^{-2}$, 400°C)(d) D5-500 ($5 \times 10^{16} \text{ cm}^{-2}$, 500°C)(e) D2-400 ($2 \times 10^{16} \text{ cm}^{-2}$, 400°C)(f) D2-500 ($2 \times 10^{16} \text{ cm}^{-2}$, 500°C)

FIG. 1. TEM images of samples obtained at higher ion implantation doses ($2 \times 10^{16} \text{ cm}^{-2}$ and $5 \times 10^{16} \text{ cm}^{-2}$) at room temperature and at annealing temperatures of 300, 400, and 500°C .

correct physical model should be established to analyze the I_s and I_c ellipsometric parameters. In the case of multi-layer systems with implanted nanoparticles, the numerical inversion of ellipsometric equations is difficult. A specific model was thus developed to take into account the rather complex sample structure.

2. Optical model

As shown in Fig. 1, the concentration of the Ag-NPs varies with depth; as a consequence, the optical properties in this layer also vary with depth. For this reason, it is important to take into account these variations in the modeling of the ellipsometric data. Therefore, the layer was divided into p sub-layers with equal thickness t_0 ($p = 30$ and $t_0 = 8.3 \text{ nm}$), namely, sub-layer 1, sub-layer 2, ..., sublayer p starting from the surface. Each sub-layer is thin enough, to consider the effective optical properties as constant.

The volume fraction (f) of Ag-NPs was determined for each sub-layer by considering that f varies according to a

Gaussian or bi-Gaussian gradient distributions. The variation of f is thus given by the following equations:

$$f(t) = A_1 e^{-0.5 \left(\frac{t-t_{m1}}{\sigma_{t1}} \right)^2} + A_2 e^{-0.5 \left(\frac{t-t_{m2}}{\sigma_{t2}} \right)^2}, \quad (3)$$

for 2 and 5 sample sets obtained at 2×10^{16} and $5 \times 10^{16} \text{ cm}^{-2}$ doses, respectively. And

$$f(t) = A_1 e^{-0.5 \left(\frac{t-t_{m1}}{\sigma_{t1}} \right)^2} \quad (4)$$

for the 1 sample set obtained at the dose of $1 \times 10^{16} \text{ cm}^{-2}$, where t is the film depth. t_{mi} , σ_{ti} , and A_i are the depth where the concentration of NPs is maximum, the standard deviation, and the amplitude of the i th Gaussian term, respectively. The schematic of the developed model is given in Fig. 4. The choice (Gaussian or bi-Gaussian) was primarily motivated by the RBS measurements and the fit quality between the ellipsometric experimental data and the optical model. The dielectric function of each sublayer is described by the shape-distributed effective medium theory (SDEMT).

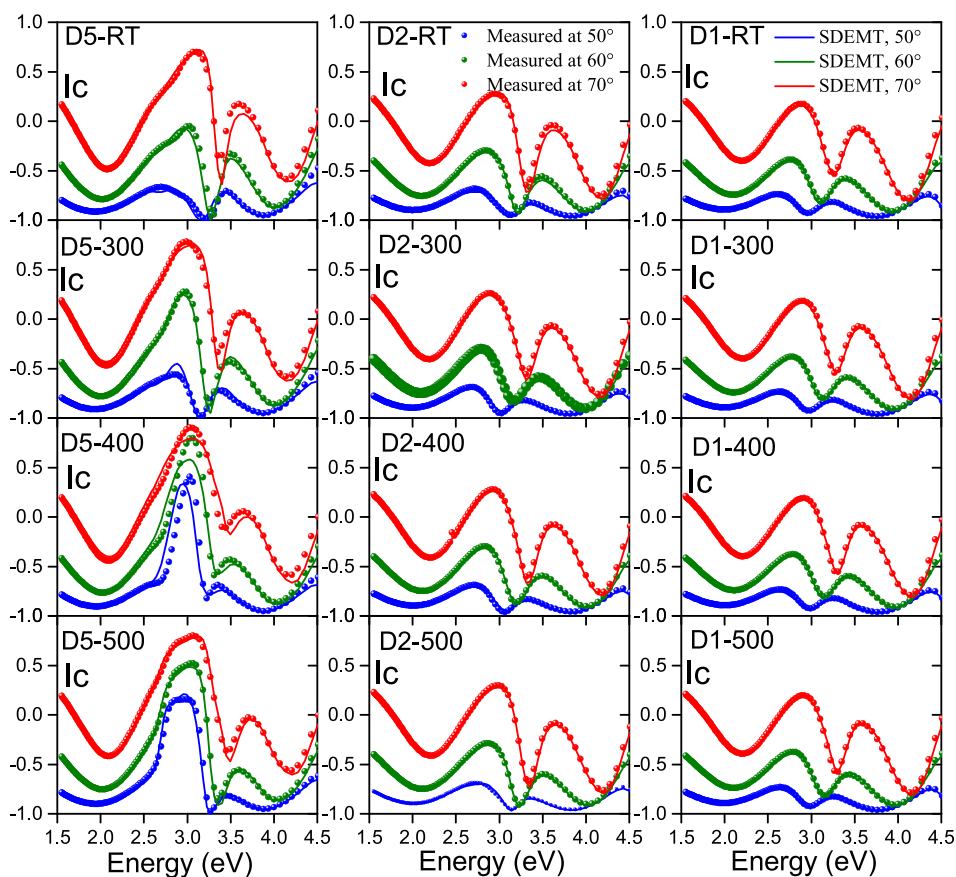


FIG. 2. Measured I_c ellipsometric parameter of D5-RT, D2-RT, D1-RT, D5-300, D2-300, D1-300, D5-400, D1-400, D5-500, D2-500, and D1-500 samples. The measurements (symbol) are performed at angles of incidence of 50°, 60°, and 70°. Calculated I_c parameter (solid line) using the SDEMT model is also given.

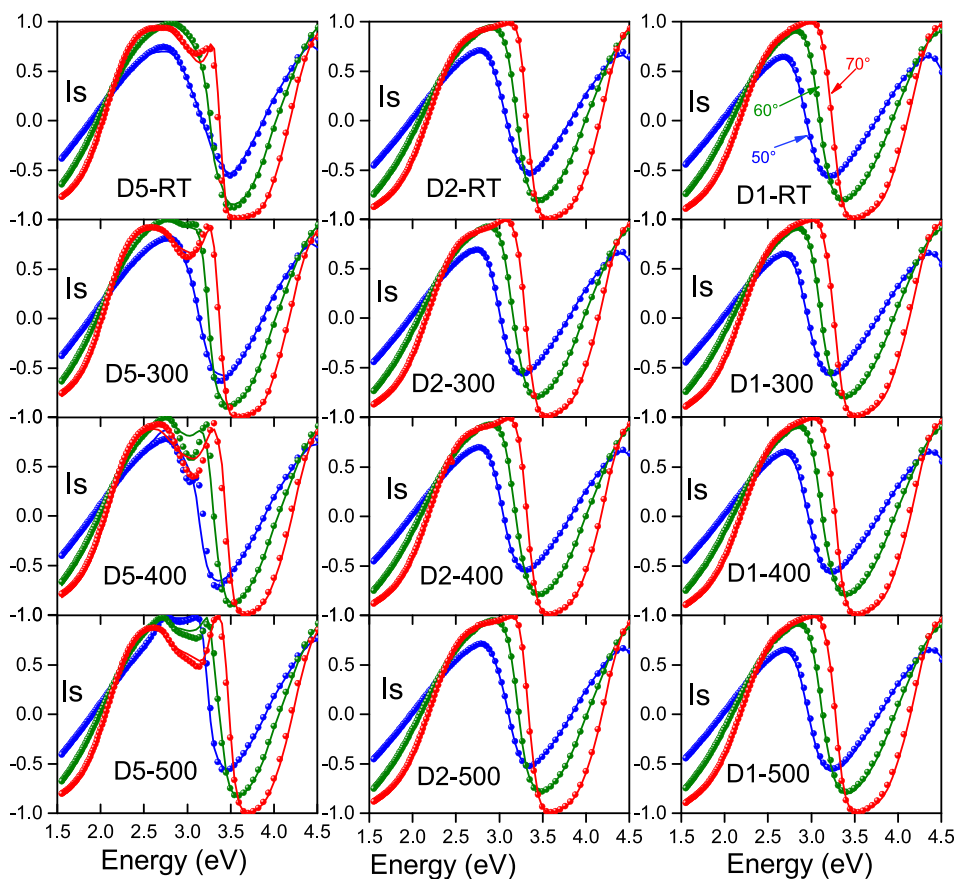


FIG. 3. Measured I_s ellipsometric parameter of D5-RT, D2-RT, D1-RT, D5-300, D2-300, D1-300, D5-400, D2-400, D1-400, D5-500, D2-500, and D1-500 samples. The measurements (symbol) are performed at angles of incidence of 50°, 60°, and 70°. The calculated I_s parameter (solid line) using the SDEMT model is also given.

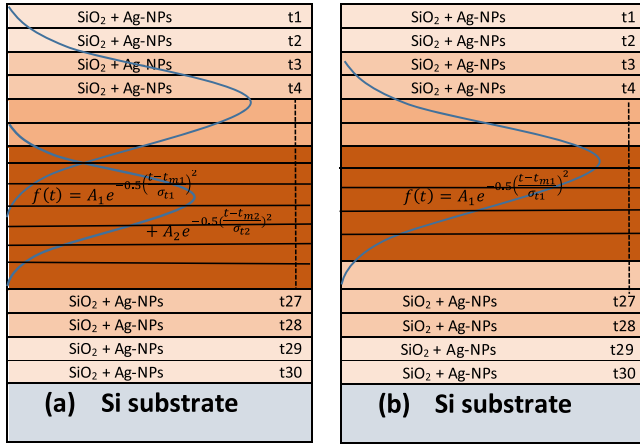


FIG. 4. The optical model used in the ellipsometric data analysis for (a) the D2 and D5 sample sets and for (b) the D1 sample set. The number of sublayers was gradually increased in the model until a very good agreement is obtained between the measured and calculated spectra.

This theory is described in our previous publications.^{9–11} The effective dielectric function (ϵ_{eff}) of a medium composed of ellipsoidal NPs embedded in a dielectric matrix is given by

$$\epsilon_{eff} = \frac{(1-f)\epsilon_m + f\beta\epsilon_{np}}{(1-f) + f\beta}, \quad (5)$$

where ϵ_{np} and ϵ_m are the complex dielectric function of the NPs and the matrix, respectively. The coefficient $\langle\beta\rangle$ is given by¹⁰

$$\langle\beta\rangle = \frac{\epsilon_m}{3} \int \int P(L_1, L_2) \sum_{i=1}^3 \frac{1}{\epsilon_m + L_i(\epsilon_{np} - \epsilon_m)} dL_1 dL_2. \quad (6)$$

Here, L_1 , L_2 , and L_3 are the depolarization parameters of ellipsoidal NPs along their three principal axes. These parameters which depend on the NP shape vary in the 0–1 range and must respect the following sum rule:

$$1 = L_1 + L_2 + L_3. \quad (7)$$

The distribution of the depolarization parameters $P(L_1, L_2)$ is introduced into Eq. (6) to take into account the NP shape distribution. We assume that the depolarization parameters follow a Gaussian distribution^{9,17}

$$P(L_1, L_2) = C e^{-0.5 \left(\frac{(L_1 - \bar{L}_1)^2}{\sigma^2} + \frac{(L_2 - \bar{L}_2)^2}{\sigma^2} + \frac{(L_3 - \bar{L}_3)^2}{\sigma^2} \right)}, \quad (8)$$

where \bar{L}_1 , \bar{L}_2 , \bar{L}_3 , and σ are the mean values and the standard deviation of the depolarization parameters, respectively, and C is a normalization constant.

The comparison between the measured spectroscopic ellipsometric spectra and the calculated ones from the proposed model is given in Figs. 2 and 3. The theoretical ellipsometric parameters (I_s , I_c) are calculated from the transfer matrix formalism¹⁶ by considering each sublayer as a mixture of Ag-NPs and SiO₂. The composite film is described by the SDEMT model as described above. The unknown fitted parameters for the D2 and D5 sample sets are those of the distributions of volume fraction (A_1 , A_2 , t_{m1} , t_{m2} , σ_{t1} , and σ_{t2}),

the mean values (\bar{L}_1 and \bar{L}_2), and standard deviation (σ) of the distribution of depolarization factors. For the D1 sample set, only the parameters A_1 , t_{m1} , σ_{t1} , \bar{L}_1 , \bar{L}_2 , and σ were considered in the fitting. The data fit was carried out simultaneously on incident angles of 50°, 60°, and 70° to improve the quality of the data fit. Since the best fit is obtained, the unknown parameters were extracted using the Levenberg-Marquardt algorithm.^{18,19} A good agreement was obtained between the experimental spectra and the calculated ones as can be seen in Figs. 2 and 3. The root mean square error between the experimental and the simulated data does not exceed 1% for all films, confirming the correctness of this model. The physical results obtained by this model are detailed below.

III. RESULTS AND DISCUSSION

A. Volume fraction of NPs

The distribution curves of the volume fraction obtained by the SDEMT model from ellipsometric data modeling for all samples are given in Fig. 5. For an easy qualitative comparison, these curves are plotted on the corresponding TEM images of the Ag-NP films.

This figure reveals that the SDEMT model effectively reproduces the distribution of the NPs concentration in the depth of the SiO₂ layer. We would like to point out here that ellipsometry presents a significant advantage as compared to TEM for the analysis of the distribution of NPs, which is the larger number of probed NPs. Indeed, by considering the ellipsometric beam diameter (3 mm), the film thickness (250 nm), and the NP mean volume fraction (2%), we can estimate that the light beam probes approximately more than 10¹⁰ NPs. Moreover, contrary to SDEMT modeling which can be extended to very small NPs, actual TEM instruments have a detection limit of 1 nm in radius. For this, the observation of the NPs by TEM might become more difficult for some samples such as D1–400 and D1–500. Therefore, modeling ellipsometric data by SDEMT provides valuable information about the distribution of NPs in the SiO₂ layer. Since the distributions of the NP volume fractions as a function of the film depth are known (Fig. 5), the mean values of the volume fractions of NPs (f_0) through the entire film thickness can be calculated from the distribution of the volume fraction deduced from the SDEMT model for each annealing temperature:

$$f_0 = \frac{1}{pt_0} \int_0^{pt_0} f(t) dt. \quad (9)$$

The evolution of f_0 with the ion implantation dose is given in Fig. 6.

As expected, Fig. 6 shows that the mean value of volume fraction (f_0) of the NPs increases with the ion dose implantation. It is also confirmed that the determined volume fraction is not influenced by annealing temperature, consistently with our previous assertion. A last point is worth to be pointed out: For all the samples, the mean values of f_0 do not exceed 2.5%. This validates *a posteriori* our SE modeling, since the SDEMT theory requires a small NP volume fraction (<30%) to neglect the interaction between the NPs.^{20–23} We note that the volume fraction of NPs in the D0.5 sample

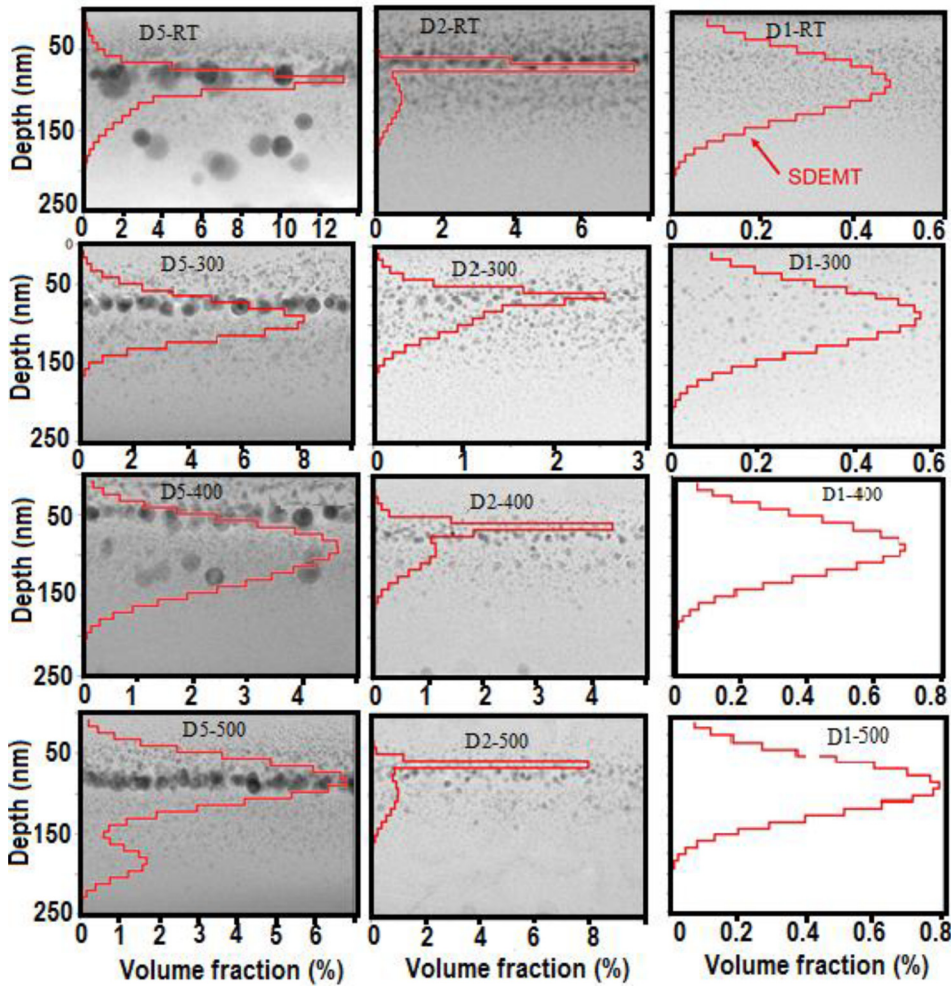


FIG. 5. Distributions of volume fraction obtained by the SDEMT model from ellipsometric data modeling. For comparison, the corresponding TEM images of Au NP films are also given.

set at a very lower ion dose of $5 \times 10^{15} \text{ cm}^{-2}$ was found to be equal to zero. This ion dose is not enough to achieve the formation of Ag-NPs with a concentration detectable by ellipsometry or TEM.

B. Distribution of NP depolarization factors

In order to obtain the shape of the NPs, we have determined the distributions of the NP depolarization factors

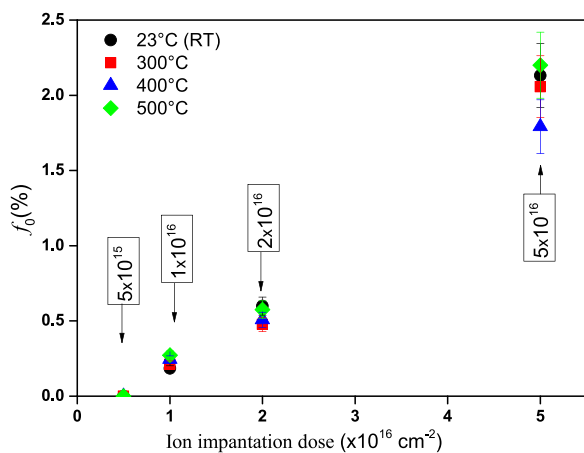


FIG. 6. The mean values of NP volume fractions through the entire film thickness as a function of ion implantation dose. The values are determined by the SDEMT model for each annealing temperature.

$P(L_1, L_2)$ by SDEMT from data ellipsometric modeling. The results are reported in Fig. 7. Overall, all samples have depolarization factor distribution centered close to $(1/3, 1/3)$, suggesting that the Ag NPs are spherical, in agreement with the TEM observation. Nevertheless, the distributions of the depolarization factors are broadened for D2 and D5 sample sets corresponding to the highest implantation doses. For the D1 sample set obtained at lower dose, the values of depolarization factors deviate from those of spherical NPs. This can be explained by the fact that these samples contain NPs of very small sizes (less than 4 nm), which induce the intrinsic confinement effect in the optical responses. Since this confinement effect is not accounted for in our model, this can explain the slight deviation of the distributions from spherical to oblates ones ($L_2=L_1$).

To quantify the variations in the NP shape distribution, we have introduced the sphericity parameter P_s

$$P_s = \sqrt{\sum_{i=1}^3 \left(\bar{L}_i - \frac{1}{3} \right)^2}. \quad (10)$$

P_s is the Euclidian distance between the center of the depolarization factor distribution and the locus of spherical NPs. It varies in the 0–0.82 range. Theoretically, the sphericity parameter of mono-dispersed spherical NPs should be equal to 0. Due to experimental scattering, this 0 value is not achievable, and we propose a more convenient sphericity

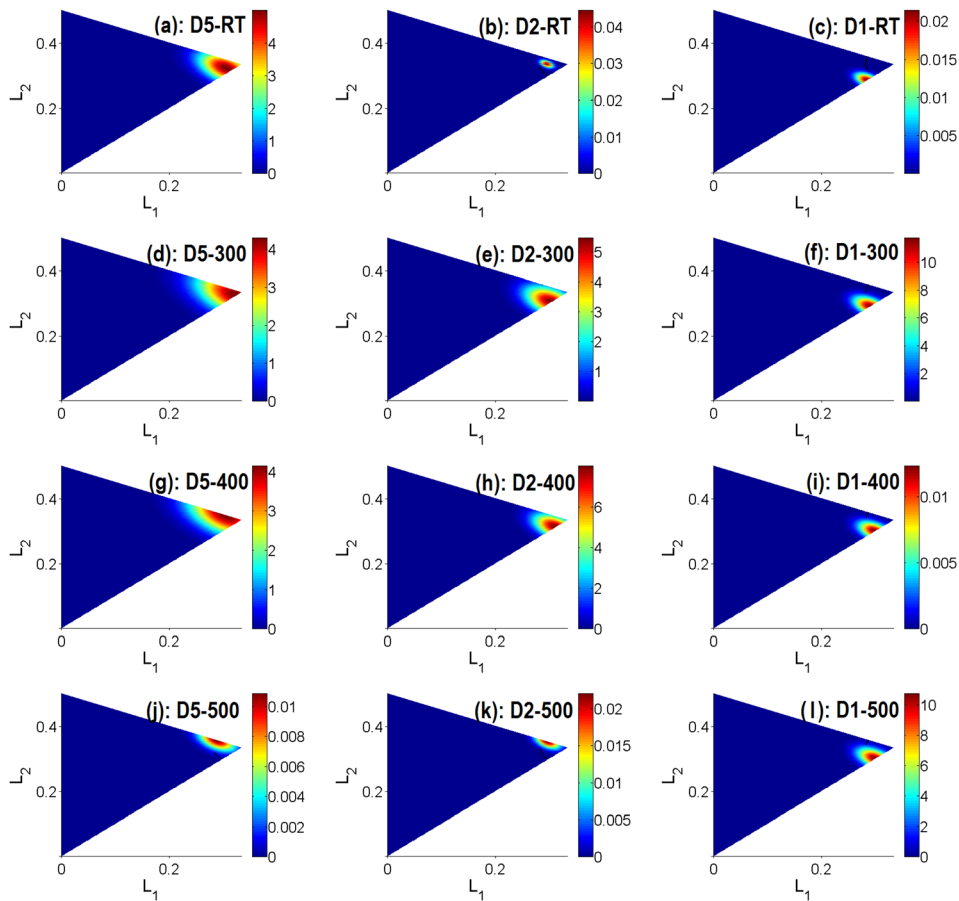


FIG. 7. Distribution of depolarization factor $P(L_1, L_2)$ of (a) D5-RT, (b) D2-RT, (c) D1-RT, (d) D5-300, (e) D2-300, (f) D1-300, (g) D5-400, (h) D2-400, (i) D1-400, (j) D5-500, (k) D2-500, and (l) D1-500 samples.

criterion obtained by comparing simulations using SDEMT and the Mie theory. It was thus found that spherical NPs with a diameter smaller than 50 nm have a sphericity parameter P_s smaller than 0.09. Following this criterion, the Ag-NPs in all samples are spherical except for the D1-RT and D1-300 samples. Indeed, Fig. 8 shows that the value of P_s is smaller than 0.09 for D1, D2, and D5 samples annealed at 400 and 500 °C, confirming the spherical character of the

NPs in these samples. The values of P_s for D1-RT and D1-300 samples containing small sizes of NPs are 0.12 and 0.11, respectively, exceeding the defined sphericity threshold. This can be attributed to the SDEMT model, which does not consider the intrinsic confinement effects appearing for a small NP radius. Moreover, the amplitude of the P_s error bars for these samples suggests that the modeling of the ellipsometric data should be improved by taking into account the confinement effects of small-sized NPs. Nevertheless, the results shown in Figs. 7 and 8 demonstrate that modeling SE data by SDEMT is a powerful way to reveal the main features of the NPs' shape distribution without the need of TEM. Finally, it is emphasized that, to avoid inaccurate characterization and to respect the limitations set by the model, the NP size (diameter) must be higher than 8 nm but smaller than 80 nm and their concentration must be smaller than 30%.

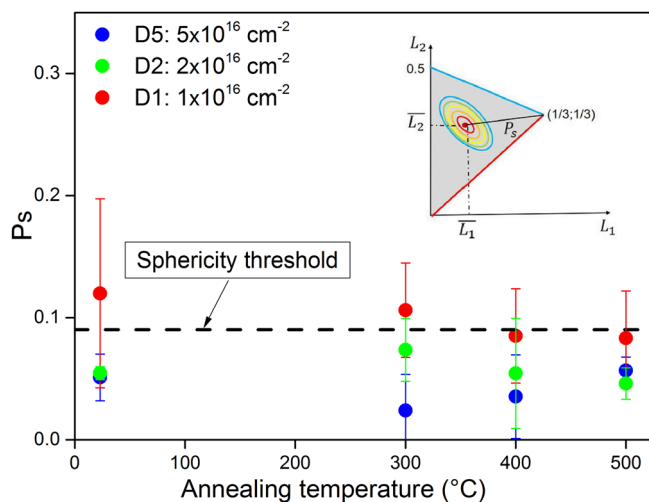


FIG. 8. Sphericity parameter (P_s) calculated by the SDEMT model for D1, D2, and D5 samples as a function of annealing temperature. The inset shows the schematic of P_s defined as the Euclidean distance between the center of the depolarization factor distribution and the locus of spherical NPs.

C. Gradient of the dielectric function in the film depth

The determination of the effective dielectric function of nanostructured film is a crucial issue to design optical devices. The variations of the real part and the imaginary part of the effective dielectric function in the film depth are depicted in Figs. 9 and 10. The imaginary part of the effective dielectric function is dominated by a plasmon band centered at around 2.85 eV, the amplitude of which increases with the implanted ion dose. According to the Fröhlich condition, this plasmon band is the optical characteristic of nearly spherical Ag NPs. In accordance with the Kramers Kronig relations, a

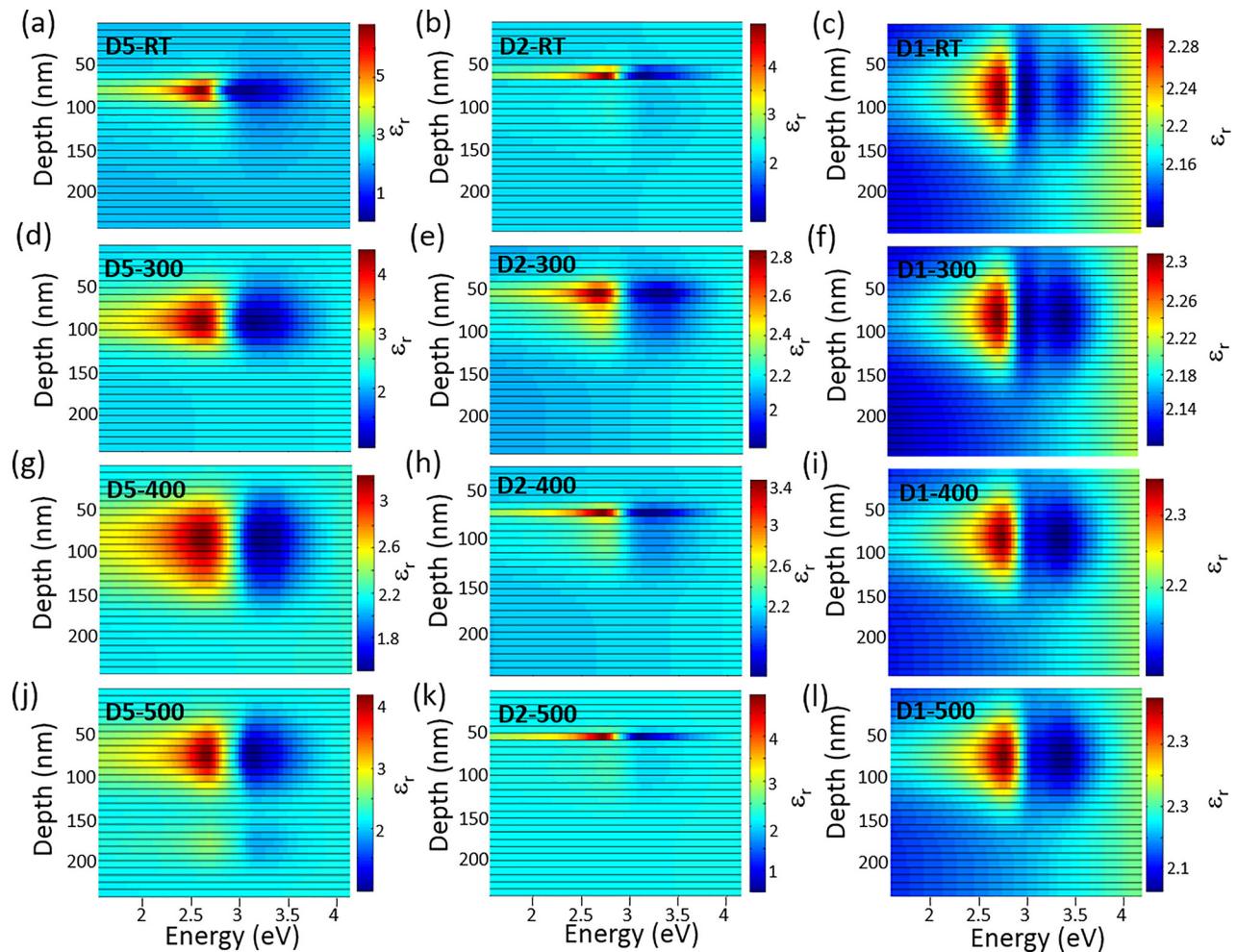


FIG. 9. Gradient of the real part of the effective dielectric function of (a) D5-RT, (b) D2-RT, (c) D1-RT, (d) D5-300, (e) D2-300, (f) D1-300, (g) D5-400, (h) D2-400, (i) D1-400, (j) D5-500, (k) D2-500, and (l) D1-500 samples.

large variation of the real part of the effective dielectric function occurs around the plasmon resonance. As expected for small NP volume fraction, the real part of the effective dielectric function at the plasmon energy is close to the dielectric function of the matrix. A comparison between TEM results and Figs. 9 and 10 also reveals that the gradient of the volume fraction in the film leads to a gradient of effective dielectric function, confirming that the latter can be used to probe the variations of the NP concentration in the film depth. Indeed, a strong localization of the plasmon resonance can be observed in the vicinity of the highly concentrated nanoparticle layer. The effective dielectric function of the D1 sample set exhibits a nearly Gaussian depth profile, while asymmetric gradient profiles can be observed in D2 and D5 sample sets. These profiles are related to two contributions, which come from the self-organized NP monolayer and the small NPs distributed in the whole film depth.

D. Absorption coefficient of the nano-composite layer

Figure 11 shows selected examples of the absorption coefficient of the nano-composite layer calculated by dividing the implanted layer into 30 sub-layers with equal thicknesses of 8.3 nm, using the transfer matrix formalism.¹⁶ For the calculation, the silicon substrate is replaced by vacuum (Fig. 11). The

plasmon band of Ag-NPs centered at around 2.85 eV is clearly observed. As expected, its amplitude increases drastically with the implanted ion dose. A typical behavior is obtained for sample D5-RT corresponding to the higher dose, whereas the samples implanted at lower doses (D2-RT and D1-RT) exhibit a large and asymmetric band. This band is attributed to the plasmonic contribution of NPs with very small sizes (less than 4 nm). These NPs exhibit an intrinsic confinement effect, which is not considered in the modeling. As can be seen in Fig. 7, the values of the depolarization factors for these samples deviate from those of spherical NPs. Therefore, in the SDEMT model, such NPs are considered as no spherical ones, and consequently, the plasmon resonance of the D1-RT and D2-RT samples exhibits strong broadening. Finally, we note that, if required, the distribution of the absorption coefficient through the film depth could be also determined as performed previously for the dielectric function (Figs. 8 and 9).

IV. CONCLUSIONS

In summary, this paper deals with the insertion of distributions of both volume fraction and depolarization factors in the modeling of the physical properties of implanted Ag-NPs in the SiO₂ layer when using spectroscopic ellipsometry characterization. This uncommon study in ellipsometry

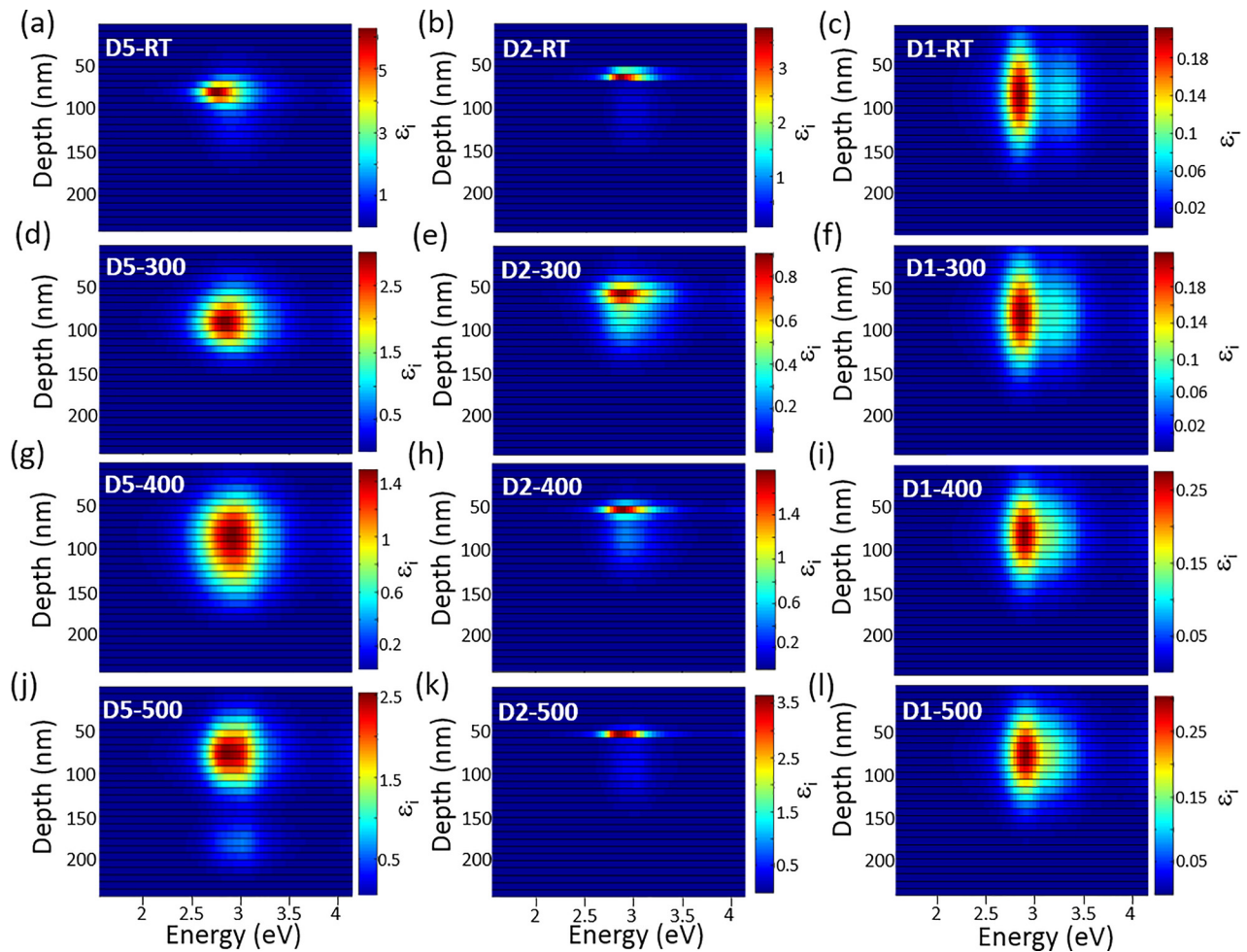


FIG. 10. Gradient of the imaginary part of the effective dielectric function of (a) D5-RT, (b) D2-RT, (c) D1-RT, (d) D5-300, (e) D2-300, (f) D1-300, (g) D5-400, (h) D2-400, (i) D1-400, (j) D5-500, (k) D2-500, and (l) D1-500 samples.

involved non-conventional calculation capabilities and specially design hardware based on shape distribution effective medium theory (SDEMT). We have demonstrated that SDEMT calculations are reliable tools for the determination, from ellipsometric data, of the NP shape and volume fraction

distributions for low concentrations. Compared to local characterization tools such as TEM, the advantage of ellipsometry combined with SDEMT is that a very large number of NPs is analyzed. Therefore, the method gives a relevant estimation of distributions of both volume fraction and depolarization factors since it directly probes a few million NPs. In addition, a gradient of the dielectric function of the nano-composite material is determined as a function of the layer depth. The results infer strong evidence that the gradient of the volume fraction in the film leads to a gradient of the effective dielectric function, confirming that the latter can be used to probe the variations of the NP concentration in the film depth. It has also been shown that the amplitude of the resonance plasmonic band is highly correlated with the implanted ion dose. The dielectric function shows a large variation in the vicinity of plasmon resonance in accordance with the Kramers-Kronig equations.

ACKNOWLEDGMENTS

The authors thank A. Resano-Garcia (LCP-A2MC, Metz) for TEM measurements.

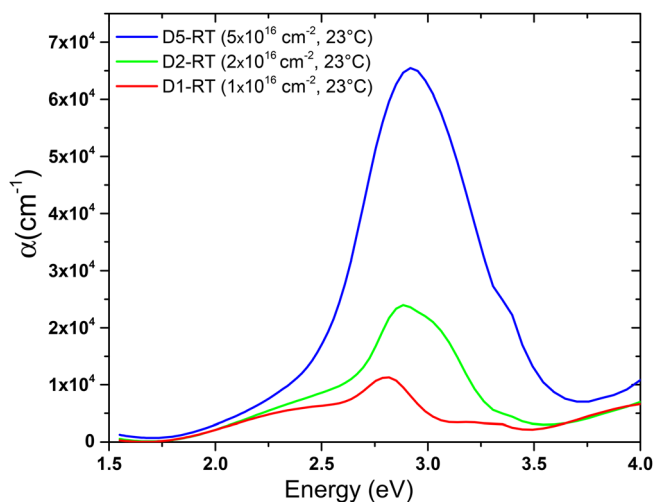


FIG. 11. Selected examples of the calculated absorption coefficient of the nano-composite layers obtained at doses of 1×10^{16} , 2×10^{16} , and 5×10^{16} ions cm^{-2} .

¹J. Z. Zhang, *Optical Properties and Spectroscopy of Nanomaterials* (World Scientific Publishing London, 2009).

- ²A. L. Stepanov, "Synthesis of silver nanoparticles in dielectric matrix by ion implantation: A review," *Rev. Adv. Mater. Sci.* **26**, 1 (2010).
- ³Y. Tan, Y. Li, and D. Zhu, in *Encyclopedia of Nanoscience and Nanotechnology*, edited by H. S. Nalwa (American Scientific Publishers, 2004), Vol. 8.
- ⁴K. Fukumi, A. Chayahara, K. Kadono, T. Sakaguchi, Y. Horino, M. Miya, K. Fujii, J. Hayakawa, and M. Satou, "Gold nanoparticles ion implanted in glass with enhanced nonlinear optical properties," *J. Appl. Phys.* **75**, 3075 (1994).
- ⁵X. H. Xiao, F. Ren, J. B. Wang, C. Liu, and C. Z. Jiang, "Formation of aligned silver nanoparticles by ion implantation," *Mater. Lett.* **61**, 4435 (2007).
- ⁶M. Dubiel, H. Hofmeister, and E. Wendler, "Formation of nanoparticles in soda-lime glasses by single and double ion implantation," *J. Non-Cryst. Solids* **354**, 607 (2008).
- ⁷A. L. Stepanov and R. I. Khaibullin, "Optics of metal nanoparticles fabricated in organic matrix by ion implantation," *Rev. Adv. Mater. Sci.* **7**, 108 (2004).
- ⁸J. F. Ziegler, J. P. Biersack, and U. Littmark, *The Stopping and Ranges of Ions in Solids* (Pergamon, New York, 1985).
- ⁹Y. Battie, A. Resano-Garcia, A. En Naciri, S. Akil, and N. Chaoui, "Determination of morphological characteristics of metallic nanoparticles based on modified Maxwell-Garnett fitting of optical responses," *Appl. Phys. Lett.* **107**, 143104 (2015).
- ¹⁰A. Resano-Garcia, Y. Battie, A. En Naciri, S. Akil, and N. Chaoui, "Experimental and theoretical determination of the plasmonic responses and shape distribution of colloidal metallic nanoparticles," *J. Chem. Phys.* **142**, 134108 (2015).
- ¹¹A. Resano-Garcia, Y. Battie, A. En Naciri, and N. Chaoui, "Interaction of a converging laser beam with a Ag colloidal solution during the ablation of a Ag target in water," *Nanotechnology* **27**, 215705 (2016).
- ¹²Y. Battie, I. Izquierdo-Lorenzo, A. Resano-Garcia, A. En Naciri, S. Akil, and P. M. Adam, "How to determine the morphology of plasmonic nanocrystals without transmission electron microscopy?," *J. Nanopart. Res.* **18**, 217 (2016).
- ¹³I. M. Lifshitz and V. V. Slyozov, "The kinetics of precipitation from supersaturated solid solutions," *J. Phys. Chem. Solids* **19**, 35 (1961).
- ¹⁴C. Wagner, "Theory of precipitate change by redissolution," *Z. Elektrochem.* **65**, 581 (1961).
- ¹⁵V. A. Borodin, K.-H. Heinig, and S. Reiss, "Self-organization kinetics in finite precipitate ensembles during coarsening," *Phys. Rev. B* **56**, 5332 (1997).
- ¹⁶R. M. A. Azzam and N. M. Bashara, *Ellipsometric and Polarized Light* (North-Holland, Amsterdam, 1977).
- ¹⁷Y. Battie, A. En Naciri, W. Chamorro, and D. Horwat, "Generalized effective medium theory to extract the optical properties of two-dimensional nonspherical metallic nanoparticle layers," *J. Phys. Chem. C* **118**, 4899 (2014).
- ¹⁸K. A. Levenberg, "A method for the solution of certain of no-linear problems in least squares," *Quart. Appl. Math.* **2**, 164 (1944).
- ¹⁹D. W. Marquardt, "An algorithm for least-squares estimation of nonlinear parameters," *J. Soc. Indust. Appl. Math.* **11**, 431 (1963).
- ²⁰A. B. Evlyukhin, C. Reinhardt, U. U. Zywiets, and B. N. Chichkov, "Collective resonances in metal nanoparticle arrays with dipole-quadrupole interactions," *Phys. Rev. B* **85**, 245411 (2012).
- ²¹U. Hohenester and J. Krenn, "Surface plasmon resonances of single and coupled metallic nanoparticles: A boundary integral method approach," *Phys. Rev. B* **72**, 195429 (2005).
- ²²M. Ranjan, "Predicting plasmonic coupling with Mie-Gans theory in silver nanoparticle arrays," *J. Nanopart. Res.* **15**, 1908 (2013).
- ²³B. B. Yousif and A. S. Samra, "Optical responses of plasmonic gold nano-antennas through numerical simulation," *J. Nanopart. Res.* **15**, 1341 (2013).